Appl. Phys. A 55, 121–134 (1992)

Applied Physics A Solids and Surfaces

Gold and Platinum Diffusion: The Key to the Understanding of Intrinsic Point Defect Behavior in Silicon

H. Zimmermann* and H. Ryssel**

Lehrstuhl für Elektronische Bauelemente, Universität Erlangen-Nürnberg, Cauerstrasse 6, W-8520 Erlangen, Fed. Rep. Germany

Received 17 December 1991/Accepted 24 February 1992

Abstract. The study of gold and platinum diffusion is found to allow the separate observation of the intrinsic point defects, i.e., of silicon self-interstitials and of vacancies. The diffusion of gold in float zone (FZ) silicon is found to be dominated by the kick-out mechanism for temperatures of 800° C and higher. The diffusion of platinum in FZ silicon is described by the kick-out mechanism for temperatures above approximately 900° C, whereas for temperatures below approximately 850° C the dissociative mechanism governs platinum diffusion. As a result of numerical simulations, we suggest a complete and consistent set of parameters which describes the diffusion of platinum in silicon in the temperature range from 700° C to 950° C and the diffusion of gold in the temperature range from 800° C to 1100° C. The generation or recombination of self-interstitials and vacancies is found to be ineffective at least below 850° C. The concentration of substitutional platinum is determined by the initial concentration of vacancies at diffusion temperatures below 850° C. Platinum diffusion below 850° C can be used to measure vacancy distributions in silicon quantitatively.

PACS: 61.70.Bv, 66.30.Jw, 61.70.Wp, 81.60.Cp

In the literature, a considerable degree of uncertainty exists about the diffusion coefficients of self-interstitials and of vacancies, respectively, and about their equilibrium concentrations. Reported values for the equilibrium concentration of self-interstitials differ by up to eight orders of magnitude at 800° C [1–5] and only a few crude estimates exist for the equilibrium concentration of vacancies [2, 6], although many attempts were carried out to determine the point defect parameters with the help of fast diffusing species. Gold diffusion was investigated extensively [7–15], whereas, only a few measurements of diffused platinum profiles have been reported so far [16–18]. In all of these experiments, however, diffusion of point-defects from the bulk to the wafer surfaces, or vice versa, took place.

In this article, a theoretical study of the kick-out diffusion mechanism [19] (which involves self-interstitials) and of the Frank-Turnbull [20] or dissociative diffusion mechanism (which involves vacancies) will show that low diffusion temperatures are the key to the determination of point defect parameters. At low temperatures, diffusion of point-defects from the bulk to the surface or vice versa, can be suppressed. Platinum will be introduced to reveal the behavior of vacancies at low temperatures. Gold diffusion profiles, which are clearly dominated by the influence of self-interstitials, allow the exclusion of the kick-out mechanism in the description of the measured platinum diffusion profiles at low temperatures. These platinum profiles, therefore, can be described by the influence of vacancies alone.

It is well accepted that self-interstitials and vacancies are both present in silicon [21–26]. But in the literature, there is not only a large uncertainty about point defect parameters but also about the generation and recombination of self-interstitials and vacancies. It will be shown here that generation and recombination of self-interstitials and vacancies is rather inefficient below approximately 850° C. Furthermore, it was not known below which temperature point-defects are existing in

* Now at: Duke University, School of Engineering, Dept. of Mechanical Engineering and Materials Science, Durham, NC 27706, USA

** Also: Fraunhofer-Arbeitsgruppe für Integrierte Schaltungen, Artilleriestrasse 12, W-8520 Erlangen, Fed. Rep. Germany

non-equilibrium concentrations. Our results will show that vacancies are present in non-equilibrium concentrations below approximately 850° C, whereas self-interstitials seem to be characterized by their equilibrium concentration still at low temperatures of approximately 800° C.

As a further result of our work, we present a complete and consistent set of parameters, including the equilibrium concentrations and diffusion coefficients of silicon self-interstitials and vacancies, for the numerical modeling of gold and platinum diffusion in silicon. With the obtained value for the equilibrium concentration of vacancies it is possible to calculate vacancy distributions in silicon quantitatively from measured platinum diffusion profiles.

1 Experimental

P-type, boron doped, float zone, dislocation free, ⟨100⟩ oriented silicon wafers were used in all experiments. They were polished at one surface. At least 30 nm of gold were deposited by evaporation after a standard cleaning procedure using Caro's acid and a dip in fluoric acid (10%). Other wafers were cleaned similarly and a platinum containing solution was spun on [27]. For the formation of a pure platinum film, the wafers were then heated at 250° C for 20 minutes. Subsequently, the platinum diffusions were performed in a furnace either at 700° C, 770° C, 850° C, 900° C, or 950° C. Gold was diffused in another furnace at 800° C or 900° C. The nitrogen flow was 10 to 11 liters per minute during platinum diffusion and 100 liters per hour during gold diffusion, respectively. The temperature was measured with Pt/PtRh thermo couples and recorded during the diffusions. The furnaces were preheated, i.e., they were at the desired temperature before loading the samples. During loading, the temperature dropped considerably. After loading, the temperature increased relatively slow in the gold furnace. Ten minutes after loading the preheated furnace, the temperatures were still approximately 20° C below the desired temperatures [28]. After 27 minutes the deviation from the desired temperatures finally was lower than 1° C. The platinum furnace heated much faster. The deviation from the desired temperature was smaller than 1° C already after 5 minutes and then held constant within ±1° C during the diffusions. After diffusion, the wafers were quenched in air. The resistivity of the wafers was 20 to 30 Ωcm for the 700° C platinum samples, 1 to 2.5 Ωcm for the 770° C and 850° C platinum samples, and 4 to 6 Ωcm for the 900° C and 950° C platinum samples, respectively. The resistivity of the wafers used for gold diffusion was 20 to 30 Ωcm for the 800° C samples and 1 to 2 Ωcm for the 900° C samples. After the diffusion, the remaining gold or platinum was removed with *aqua regia*.

Platinum and gold profiles were determined using deep level transient spectroscopy (DLTS) measurements. Two preparation methods were applied. In the first, samples of approximately 1 cm² were bevelled under an angle of 1°08′ or 2°52′. To remove the damage caused by mechanical polishing, approximately 15 μm of silicon were etched off with an $HF/HNO_3/CH_3COOH$ mixture. In the second method, steps of various height (0.5 to 20 μm) were etched into the samples. Immediately after a further HF dip, Schottky contacts were deposited by evaporation of hafnium at a pressure of less than 2×10^{-6} torr. For both preparation methods, the doping concentration was determined by capacitance voltage (C/V) measurements for each Schottky contact [29]. The concentration of the gold or platinum donor level then was measured by DLTS [30]. The energetic position of the platinum donor level was determined to be 0.330 eV above the valence band in silicon, which is in good agreement with the values given in the literature [31–33]. The gold donor level lay 0.327 eV above the valence band, which is also in good accordance to the literature values [34–36].

2 Theory

2.1 Reactions Between Metal Atoms, Vacancies, and Self-Interstitials

The dissociative diffusion mechanism was suggested by Frank and Turnbull to describe the diffusion of Cu in Ge [20]. The corresponding reaction for an interstitial metal atom (M_i), which occupies a vacancy (V) and forms a substitutional metal atom (M_s), leads to:

$$M_i + V \underset{k_{-1}}{\overset{k_{+1}}{\Leftrightarrow}} M_s . \tag{1}$$

The kick-out mechanism suggested by Gösele is characterized by the generation of a self-interstitial (I), when the substitutional metal atom configuration is formed [19]:

$$M_i \underset{k_{-2}}{\overset{k_{+2}}{\Leftrightarrow}} M_s + I . \tag{2}$$

The symbols k_{+1}, k_{-1}, k_{+2}, and k_{-2} are the reaction constants in forward and reverse direction, respectively.

The generation and recombination of self-interstitials and vacancies can be described by the reaction (0 = undisturbed lattice)

$$I + V \Leftrightarrow 0 , \tag{3}$$

which is generally characterized by the generation/recombination constant or so-called bulk recombination rate K_B. In the undisturbed lattice, the point defect concentrations are equal to their equilibrium concentrations C_I^* and C_V^*. The generation/recombination term for self-interstitials and vacancies accordingly can be written as $-K_B(C_I C_V - C_I^* C_V^*)$ [37–39] [compare (14) and (15)].

2.2 Dissociative Mechanism

The reaction (1) produces the following equations for the dissociative mechanism, when the generation or annihil-

ation of vacancies is taken into account [40]:

$$\frac{\partial C_s}{\partial t} = k_{+1} C_i C_V - k_{-1} C_s, \tag{4}$$

$$\frac{\partial C_i}{\partial t} = \operatorname{div} D_i \operatorname{grad} C_i - k_{+1} C_i C_V + k_{-1} C_s, \tag{5}$$

$$\frac{\partial C_V}{\partial t} = \operatorname{div} D_V \operatorname{grad} C_V - k_{+1} C_i C_V + k_{-1} C_s - K_V (C_V - C_V^*). \tag{6}$$

In these equations, C and D are used to denote concentrations and diffusion coefficients. The indices s, i, and V refer to substitutional metal atoms, interstitial metal atoms, and vacancies, respectively. C_V^* is the equilibrium concentration of vacancies. In deriving (4), it is assumed that substitutional metal atoms possess a negligible diffusion coefficient.

The generation/recombination term $K_V(C_V - C_V^*)$ in (6) allows the inclusion of dislocations [41] and/or swirls [42] as vacancy sources or sinks. K_V determines the speed of vacancy generation or annihilation due to these defects. Vacancies are generated for $C_V < C_V^*$ and annihilated for $C_V > C_V^*$. In the cases of absence or ineffectiveness of these defects, K_V may be used to estimate an upper boundary for the generation or recombination of self-interstitials and vacancies (see Sects. 2.4 and 3.2.2).

The reaction rate k_{-1} can be eliminated using the principle of detailed balance[1] for the dissociative mechanism. This assumption results in

$$k_{-1} = k_{+1} C_i^* C_V^* / C_s^*, \tag{7}$$

with the equilibrium concentrations C_i^* and C_s^* for interstitial (i) and substitutional (s) metal atoms, respectively. C_s^* represents the concentration of substitutional metal atoms at the surface according to [14].

2.3 Kick-out Mechanism

Reaction (2) results in the following set of differential equations for the kick-out mechanism [19]:

$$\frac{\partial C_s}{\partial t} = k_{+2} C_i - k_{-2} C_s C_I, \tag{8}$$

$$\frac{\partial C_i}{\partial t} = \operatorname{div} D_i \operatorname{grad} C_i - k_{+2} C_i + k_{-2} C_s C_I, \tag{9}$$

$$\frac{\partial C_I}{\partial t} = \operatorname{div} D_I \operatorname{grad} C_I + k_{+2} C_i - k_{-2} C_s C_I - K_I (C_I - C_I^*). \tag{10}$$

C_I^* stands for the equilibrium concentration of self-interstitials. Again it is assumed that substitutional metal atoms have a negligible diffusion coefficient and the reaction rate k_{-2} can be eliminated analogous to k_{-1}:

$$k_{-2} = k_{+2} C_i^* / C_s^* C_I^*. \tag{11}$$

[1] In thermal equilibrium, every process must be balanced by its exact opposite. This is called the *principle of detailed balance*

The generation/recombination term $K_I(C_I - C_I^*)$ in (10) describes the effect of dislocations [43] and/or swirls [42] as self-interstitial sources or sinks, respectively. K_I is the reaction rate for annihilation or generation of self-interstitials by these defects. If these defects are absent or ineffective this generation/recombination term may be used to include the influence of vacancies (see Sect. 2.4).

2.4 Combination of Dissociative and Kick-out Mechanism

When reactions (1) to (3) have to be considered at the same time, a set of four partial differential equations has to be solved:

$$\frac{\partial C_s}{\partial t} = k_{+1} C_i C_V - k_{-1} C_s + k_{+2} C_i - k_{-2} C_s C_I, \tag{12}$$

$$\frac{\partial C_i}{\partial t} = \operatorname{div} D_i \operatorname{grad} C_i - k_{+1} C_i C_V + k_{-1} C_s - k_{+2} C_i + k_{-2} C_s C_I, \tag{13}$$

$$\frac{\partial C_I}{\partial t} = \operatorname{div} D_I \operatorname{grad} C_I + k_{+2} C_i - k_{-2} C_s C_I - K_B (C_I C_V - C_I^* C_V^*), \tag{14}$$

$$\frac{\partial C_V}{\partial t} = \operatorname{div} D_V \operatorname{grad} C_V - k_{+1} C_i C_V + k_{-1} C_s - K_B (C_I C_V - C_I^* C_V^*). \tag{15}$$

The generation/recombination term $-K_B(C_I C_V - C_I^* C_V^*)$ of self-interstitials and vacancies in (14) and (15) can be brought into the form $-K_V(C_V - C_V^*)$ [compare (6)], when the diffusion coefficient of self-interstitials D_I is large and C_I, then, can be assumed to be equal to C_I^* and

$$K_V = K_B C_I^* \tag{16}$$

holds approximately. Another possibility would be to bring $-K_B(C_I C_V - C_I^* C_V^*)$ into the form $-K_I(C_I - C_I^*)$ [compare (10)] assuming $C_V = C_V^*$ and

$$K_I = K_B C_V^*. \tag{17}$$

However, this approximation can be excluded because $C_V = C_V^*$ does not hold at the low temperatures and for the diffusion times examined in this paper.

2.5 Initial and Boundary Conditions

Each of the above sets of Eqs. (4) to (6), (8) to (10), and (12) to (15) can be integrated using the general purpose solver PROMIS [44] for appropriate initial and boundary conditions. A concentration of 1×10^{10} cm^{-3} is assumed as initial condition for substitutional metal. The initial concentration of interstitial metal is arbitrarily assumed to be 1×10^9 cm^{-3}. The results of the simulations, however, do not depend at all on these values for $C_s(t=0)$ and $C_i(t=0)$, because they are orders of magnitudes lower than after the diffusion. The equilibrium concentration of self-interstitials at the corresponding diffusion temperature is taken for $C_I(t=0)$ [45]. This assumption seems

justified, because according to reaction (2), a very large supersaturation of self-interstitials builds up in the bulk when substitutional metal is formed. The initial concentration of self-interstitials is not important as long as it is much smaller than the metal concentration. This condition is fulfilled for our experiments. Gold diffusion experiments also showed that the self-interstitial diffusion coefficient D_I is very large. Therefore, the surface value C_I^* and not the initial self-interstitial concentration governs the self-interstitial behavior in the bulk already after a few minutes of diffusion.

It will, however, be shown that vacancies are not necessarily present in their equilibrium concentration during thermal processing at relatively low temperatures, because the generation/recombination rate K_B, respectively K_V, then is small. Therefore, a value $C_V(t=0) \neq C_V^*$ has to be chosen as initial condition.

Interstitial gold or platinum diffused from an infinite source from the surface of the wafer. Therefore, $C_i(x=0)=C_i^*$ represents a Dirichlet boundary condition for (5), (9), and (13). A Neumann boundary condition is used at the backside, because it is assumed that the platinum cannot leave the wafer there. Dirichlet boundary conditions are used for (6), (10), (14), and (15), i.e., the concentrations of self-interstitials and vacancies are assumed to be fixed at their equilibrium values at both wafer surfaces. It shall be mentioned that all four quantities, C_s, C_i, C_I, and C_V, are characterized by their equilibrium concentrations C_s^*, C_i^*, C_I^*, and C_V^*, respectively, at the wafer surface. This circumstance describes the fact that the concentration of substitutional gold and platinum at the surface is constant and equal to C_s^* for different diffusion times larger than approximately 0.5 h. For the sake of clarity it has to be noted that C_s^* is not given by a boundary condition, since (4), (8), and (12) do not contain diffusion terms. The value of C_s^* at the boundary results from the principle of detailed balance and the structure of the differential equations. The values of k_{+1}, respectively k_{+2}, determine how long it takes until the value C_s^* is reached at the surface.

2.6 Study of the Different Mechanisms

2.6.1 Dissociative Mechanism. Numerical Analysis. To illustrate the formation of substitutional metal in the bulk, (4) to (6) are solved numerically. Figure 1 shows the increase of the substitutional metal concentration in the bulk as a function of time, when metal is diffused from one surface. After approximately 5 seconds the substitutional metal concentration increases rapidly in this example. This increase in general is caused when the interstitial metal reaches the position in the bulk which is examined (in this example in the middle of the wafer). The steepness of this increase is determined by the value of the diffusion coefficient of interstitial metal and by the value of the reaction constant k_{+1}. After 10 seconds all available vacancies are occupied and the concentration of substitutional metal C_s remains constant. This region with constant C_s shall be called plateau region in the following. C_s can further increase only when new vacancies arrive

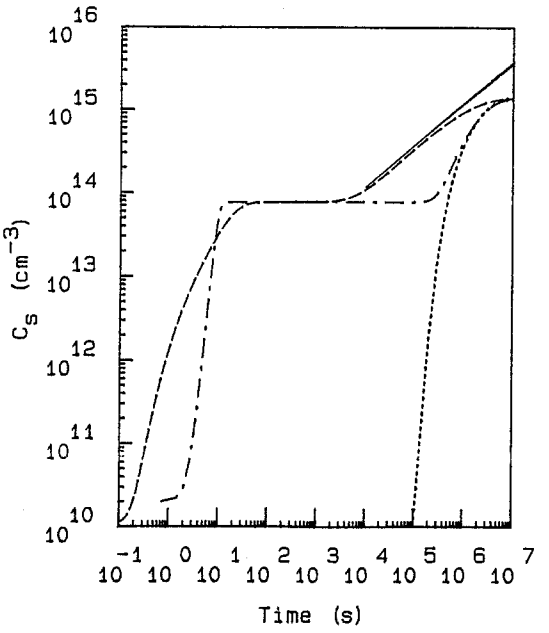

Fig. 1. Increase of substitutional metal in the bulk as a function of time ⟨(——) analytical kick-out mechanism; (- - -) simulated kick-out mechanism; (· · · · ·) analytical Frank-Turnbull mechanism; (–·–·) simulated Frank-Turnbull mechanism⟩. K_V in (6) and K_I in (10), respectively, was set to zero. The other parameters were chosen arbitrarily with $D_i \gg D_V$, $D_i C_i^* \gg D_V C_V^*$, and k_{+1} large, respectively $D_i \gg D_I$, $D_i C_i^* \gg D_I C_I^*$, and k_{+2} large. However, the same parameters were used in the analytical calculations as in the simulations

from the wafer surfaces – in this example after approximately 2×10^5 s. Finally, the increase is limited after 10^7 s.

Analytical Time Dependence for Interaction with the Wafer Surfaces. An analytical solution for the concentration of substitutional metal in the center of the wafer (d = wafer thickness, erfc = complementary error function) [46]

$$C_s\left(\frac{d}{2}, t\right) = 2C_s^* \sum_{n=0}^{\infty} (-1)^n \operatorname{erfc} \frac{(2n+1)d/2}{2(Dt)^{1/2}} \tag{18}$$

with

$$D = \frac{D_V C_V^*}{C_s^* + C_V^*} \tag{19}$$

compares well with the simulated curve (Fig. 1) only for diffusion times larger than 5×10^5 s. This fact is not surprising, because (18) was deduced for the case when diffusion of vacancies from both wafer surfaces to the center of the wafer takes place. Obviously it does not make a large difference in C_s whether the metal diffuses from one or from both wafer surfaces. Simulations affirmed this conclusion. It shall be noted that the indistinguishability between one- and both-sided diffusion relates to the fast diffusion of interstitial metal.

Analytical Analysis of the Plateau Region. Up to now, nobody else examined the plateau region (from 10 to 10^5 s in this example). However, in fact this region contains the key to the determination of the vacancy equilibrium concentration.

A relation holds in this plateau region between the initial ($C_V(t=0)$) and the equilibrium (C_V^*) concentration of vacancies [28, 47]:

$$C_V(t=0)=\frac{C_s^b}{C_s^*}(C_s^*+C_V^*). \tag{20}$$

C_s^b represents the concentration of substitutional platinum in the bulk and C_s^* is the concentration of substitutional platinum at the wafer surface, respectively. Both can be measured. In the derivation of (20), a large diffusion coefficient of interstitial metal and a large reaction constant k_{+1} were assumed. These assumptions are justified for platinum at low temperatures.

When the equilibrium concentration of vacancies is varied to obtain a best fit of the measured diffusion profiles with (12) to (15), the corresponding initial concentration of vacancies can be calculated according to Eq. (20).

When the vacancy equilibrium concentration is taken as an initial condition for platinum diffusion, C_V^* can be determined according to [28, 47]:

$$C_V^*=\frac{C_s^* C_s^b}{C_s^*-C_s^b}. \tag{21}$$

C_s^* and C_s^b can be measured. D_V can be determined by comparison of simulations with the measured profile near the surface.

After the determination of C_V^*, (20) then can be used to measure vacancy distributions $C_V(t=0,x)$ as a function of the depth x, when C_s^b is replaced by $C_s(x)$. The concentration of substitutional platinum has to be measured in various depth. Then $C_V(t=0,x)$ can be calculated according to (20). The depth x has to be chosen larger than the diffusion depth of vacancies from or to the surface during platinum diffusion. However, this does not limit the method because D_V is many orders of magnitude smaller than D_i. The depth x has only to be larger than 10 μm for a platinum diffusion temperature of 770° C, and larger than 2 μm at 700° C for a diffusion time of 4 hours, respectively. The vacancy distributions at larger depth do not change due to diffusion of vacancies from the surface. It shall be mentioned that the value of C_s^* does not limit the measurable vacancy concentration. Larger values of $C_V(t=0,x)$ than C_s^* also can be determined.

Influence of Point Defect Generation or Recombination in the Plateau Region. To account for the generation or recombination of self-interstitials and vacancies, the derivation of (20) can be modified compared to [28, 47]. The local dynamical equilibrium

$$\frac{C_V}{C_V^*}=\frac{C_s}{C_s^*} \tag{22}$$

still holds. The concentration of vacancies is, however, not only reduced by the formation of substitutional metal, but also by a generation/recombination term C_{gr}, which cannot only decrease but also increase the vacancy concentration depending on the sign of C_{gr}

$$C_V=C_V(t=0)-C_s^b+C_{gr}. \tag{23}$$

C_V can be eliminated with the aid of (22) and the concentration of substitutional metal in the bulk C_s^b can be expressed by:

$$C_s^b=\frac{C_V(t=0)+C_{gr}}{1+C_V^*/C_s^*}. \tag{24}$$

C_{gr} is given by the time integral of $-K_B(C_I C_V-C_I^* C_V^*)$. As will be shown, self-interstitials diffuse very fast. Therefore, C_I may be approximated by C_I^*. C_{gr} is positive, when $C_V<C_V^*$. In the opposite case $C_V>C_V^*$, C_{gr} is negative and the vacancy concentration and correspondingly C_s^b are reduced. The difference in the substitutional metal concentration ΔC_s^b between two observation times t_1 and t_2 with $\Delta t=t_2-t_1$ can then be calculated:

$$\Delta C_s^b=\frac{\Delta C_{gr}}{1+C_V^*/C_s^*} \tag{25}$$

with

$$\Delta C_{gr}=-K_B(C_I C_V-C_I^* C_V^*)\Delta t. \tag{25a}$$

The concentration of substitutional metal, therefore, will change with time, if the generation or recombination of self-interstitials and vacancies is effective, i.e., when C_V differs considerably from C_V^* and the bulk recombination constant K_B possesses a large value.

2.6.2 Kick-out Mechanism. Numerical Analysis. The increase of substitutional metal in the bulk as a function of diffusion time can also be seen in Fig. 1. This figure contains the solution of (8) to (10) for the same equilibrium value of substitutional metal as for the dissociative mechanism. After a steep increase, which is determined by the diffusion coefficient of the interstitial metal and by the reaction rate k_{+2}, a plateau is reached. In our example this is the case after approximately 30 s. At this time so many self-interstitials were generated by the formation of substitutional metal according to reaction (2) that the concentration of the substitutional configuration cannot increase further. After 10^4 s, the concentration of self-interstitials starts to decrease at the spatial position under observation due to out-diffusion to the wafer surfaces. With increasing time, more self-interstitials diffuse to the surfaces and the concentration of substitutional metal finally becomes limited by the equilibrium concentration of substitutional metal.

Analytical Time Dependence for Interaction with the Wafer Surfaces. Gösele et al. reported an analytical expression for the increase of substitutional metal in the center of the wafer as a function of time for the case that diffusion of self-interstitials to the wafer surfaces is possible (d = wafer thickness) [19]:

$$C_s\left(\frac{d}{2},t\right)=\frac{2}{d}(\pi C_s^* D_I C_I^* t)^{1/2}. \tag{26}$$

In an intermediate time range from 10^4 to 5×10^5 s, this expression compares well to the numerical simulation. Analog to the dissociative mechanism, there is practically no difference whether the metal diffuses from one or two surfaces. For larger times, however, (26) does not limit the increase of C_s.

Analytical Analysis for the Plateau Region. The more interesting time range, however, is the plateau. We showed that the following expression can be deduced from (8) to (10) [28, 47]:

$$C_I(t=0)=\frac{C_s^* C_I^*}{C_s^b}-C_s^b. \tag{27}$$

Analog to the dissociative mechanism, a large D_i (i.e., $C_i=C_i^*$) and a large k_{+2} were used to derive (27). If it is possible to assume the equilibrium concentration of self-interstitials as initial condition, C_I^* can be calculated from [28, 47]:

$$C_I^*=\frac{(C_s^b)^2}{C_s^*-C_s^b}. \tag{28}$$

This equation allows the determination of C_I^* directly from the concentration of substitutional metal C_s^b, which is measured in the bulk. The diffusion coefficient of self-interstitials can be obtained by simulations and comparison with the measured metal profile near the surface.

3 Results and Discussion

3.1 Gold

3.1.1 Comparison of Modeling with Experiments. In this section, measured gold diffusion profiles will be compared with results of numerical simulations. Figure 2 depicts gold profiles after diffusion at 800° C for 0.5, 2.0, and 16 h, respectively. Figure 3 shows measured results after diffusion at 900° C for the same periods. These profiles can be explained by out-diffusion of self-interstitials. Figure 4 compares the measured increase of the substitutional gold concentration in the center of the wafer at 900° C with the

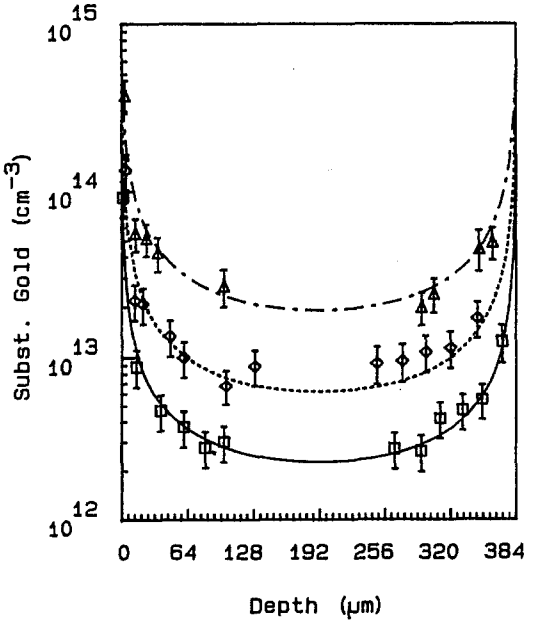

Fig. 2. Measured (□: 0.5 h, ◇: 2.0 h, △: 16.0 h) and simulated gold profiles after diffusion at 800° C ⟨(——) 0.5 h; (- - -) 2.0 h; (–·–·) 16.0 h⟩

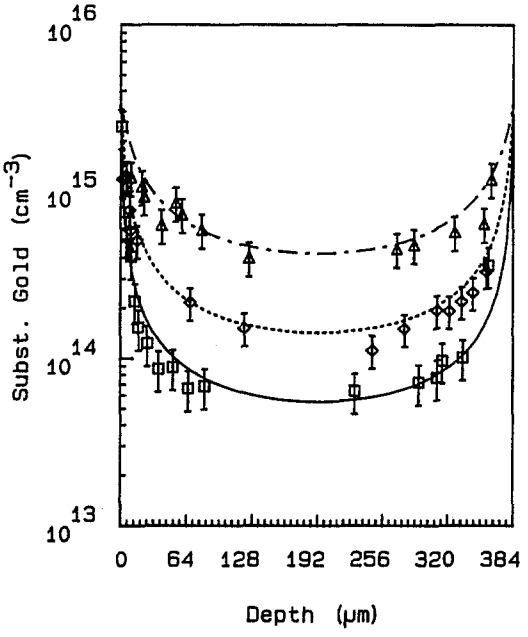

Fig. 3. Measured (□: 0.5 h, ◇: 2.0 h, △: 16.0 h) and simulated gold profiles after diffusion at 800° C ⟨(——) 0.5 h; (- - -) 2.0 h; (–·–·) 16.0 h⟩

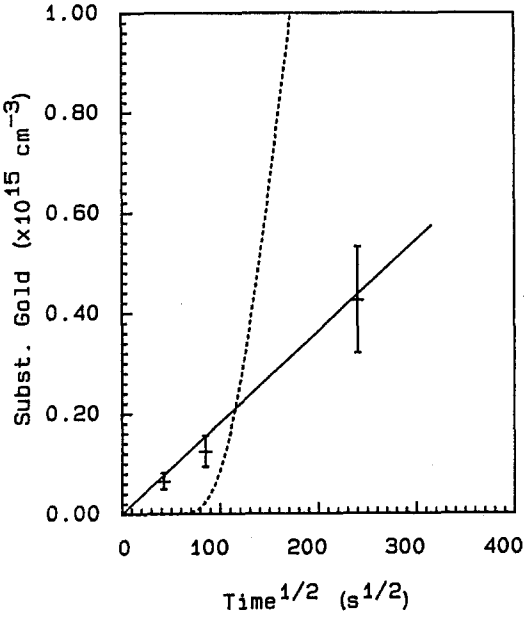

Fig. 4. Comparison of the measured bulk gold concentration with theoretical predictions (—— [solid line]: kick-out mechanism, - - - [dashed line]: Frank-Turnbull mechanism). The experimental data result from the mean values of the data points in Fig. 3, which are closest to the middle of the wafer

predictions of (18) and (26). The measured time dependence of C_s can be explained very well by (26), which was derived for the kick-out mechanism. Equation (18) leads to a much faster increase of C_s, than was measured. Vacancies, therefore, did not play an important role during these diffusion experiments. A corresponding result was found for the diffusion experiment at 800° C. Therefore, the out-diffusion of self-interstitials governs

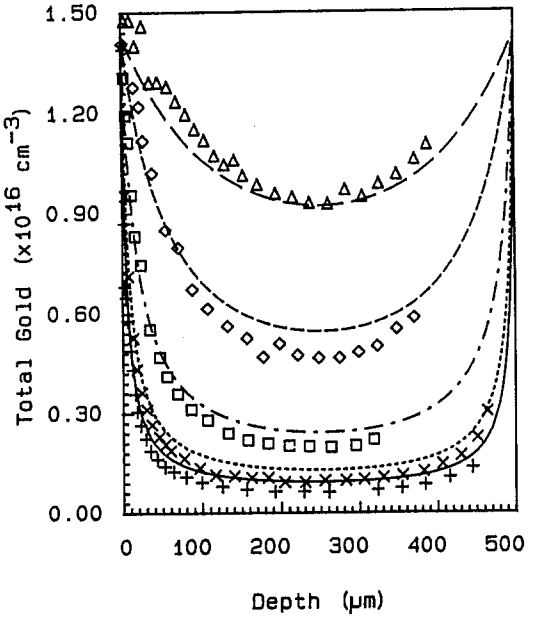

Fig. 5. Comparison of simulated gold profiles with neutron activation analysis measurements of Stolwijk [14] after diffusion at 1000° C (+: 0.467 h, ×: 1.03 h, □: 4.27 h, ◇: 26.8 h, △: 100.6 h)

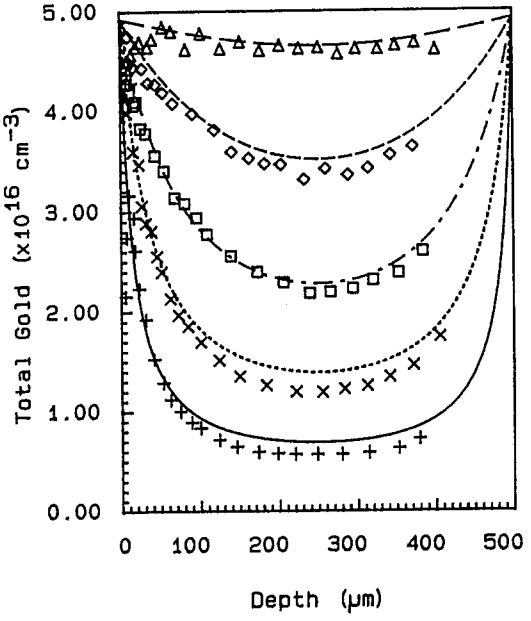

Fig. 6. Comparison of simulated gold profiles with neutron activation analysis measurements of Stolwijk ⟨13⟩ after diffusion at 1100° C (+: 0.428 h, ×: 1.97 h, □: 6.16 h, ◇: 19.8 h, △: 70.1 h)

the formation of substitutional gold even at the lowest investigated temperature of 800° C.

Numerical simulations were performed to optimize the set of parameters in (8) to (10) to obtain a best fit to our measured gold profiles (Figs. 2 and 3) and to the measurements of Stolwijk et al. at 1000 and 1100° C (Figs. 5 and 6) [14, 13]. For the temperatures of 800 and 900° C, measured temperature ramps were used in the simulations [28]. For the data of Stolwijk, the simulations were performed with constant temperatures. The sum of simulated substitutional and interstitial gold concentrations is compared to the total measured gold concentration in Figs. 5 and 6. The simulated results shown in Figs. 2, 3, 5, and 6 were obtained with the following parameters:

$$C_s^* = 3.28 \times 10^{23} \exp(-1.860\ \text{eV}/kT)\ \text{cm}^{-3}, \quad (29a)$$

$$C_i^* = 1.45 \times 10^{21} \exp(-1.729\ \text{eV}/kT)\ \text{cm}^{-3}, \quad (29b)$$

$$D_i = 9.31 \times 10^{-4} \exp(-0.261\ \text{eV}/kT)\ \text{cm}^2\ \text{s}^{-1}, \quad (29c)$$

$$C_I^* = 1.94 \times 10^{27} \exp(-3.835\ \text{eV}/kT)\ \text{cm}^{-3}, \quad (29d)$$

$$D_I = 2.58 \times 10^{-2} \exp(-0.965\ \text{eV}/kT)\ \text{cm}^2\ \text{s}^{-1}, \quad (29e)$$

$$k_{+2} = 1.00 \times 10^{22} \exp(-5.000\ \text{eV}/kT)\ \text{s}^{-1}, \quad (29f)$$

$$k_I = 0. \quad (29g)$$

C_s^* was taken from [12], the other parameters were fit. Our measured surface concentrations confirm the values of [12] within the experimental accuracy. C_i^* and D_i result in a larger product $C_i^* D_i$, than was reported by Stolwijk [14]. However, this product had to be chosen larger in order to obtain a large enough flux of interstitial gold [28]. With various splittings of the product of Stolwijk the gold concentration did not reach the measured concentrations near the reverse side of the wafers. D_i had to be increased in comparison to the value of Wilcox [8], because C_i^* could not be chosen larger than (29b). The reason is that the sum of the concentrations of substitutional and interstitial gold must not be larger than the total gold concentration given by neutron activation analysis [28]. D_I and C_I^* were fit under the constraint that their product results in the value for the product $D_I C_I^*$, which was given by Tan and Gösele [2], and that the platinum diffusion experiments have to be described with the same parameters.

The value of k_{+2} may only serve as an estimate. However, the activation energy of the reverse reaction constant k_{-2} is also positive, when (29a), (29b), (29d), and (29f) are inserted into (11). Therefore, the consistency of the set of parameters (29) can be concluded.

Morehead et al. reported that during gold diffusion, a contribution of the dissociative mechanism has to be considered above 1000° C [11]. These authors, however, performed their simulations with a simplified model using only one diffusion equation. Coffa et al. [15] explained their spreading-resistance measurements at 800 and 970° C in terms of the kick-out mechanism. The conclusion can be drawn that the simplified model obviously is not applicable, because the complete model of the kick-out mechanism describes our measurements with good success. Furthermore, from our experiments we cannot decide whether in our gold samples the vacancy concentration was smaller than approximately $3 \times 10^{12}\ \text{cm}^{-3}$ [according to (20), with $C_s^*(800°\text{ C}) = 6 \times 10^{14}\ \text{cm}^{-3}$, $C_V^* = 6 \times 10^{13}\ \text{cm}^{-3}$, and a bulk value of $C_s = 3.0 \times 10^{12}\ \text{cm}^{-3}$] or the reaction constant k_{+1} of gold for the dissociative mechanism is very small. However, in order to save computing time and because of the time dependence of the bulk concentration (Fig. 4), the assumptions of $k_{+1} = 0$ and that reaction (3) is negligible, seem to be justified. Therefore, (12) to (15) reduce to (8) to

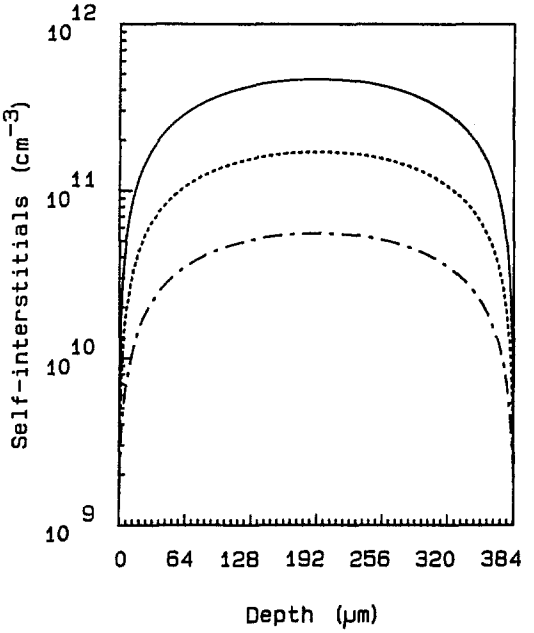

Fig. 7. Simulated self-interstitial profiles for the gold diffusions at 800° C in Fig. 2 ⟨(——) 0.5 h; (- - -) 2.0 h; (–·–·) 16.0 h⟩

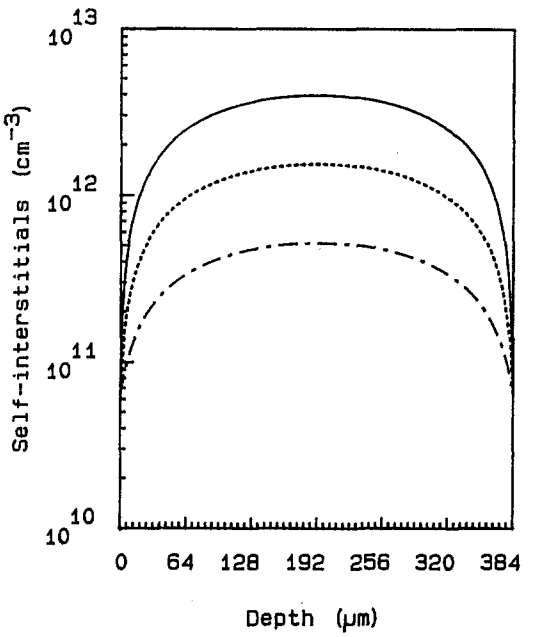

Fig. 8. Simulated self-interstitial profiles for the gold diffusions at 900° C in Fig. 2 ⟨(——) 0.5 h; (- - -) 2.0 h; (–·–·) 16.0 h⟩

(10) of the kick-out mechanism. K_I can be set to zero because the wafers were dislocation free.

The simulated gold profiles are in good accordance to our measurements. For the shortest diffusion periods, the simulated concentrations lie slightly above the measured concentrations of Stolwijk et al. This small deviation is probably caused by the constant temperatures used in the simulations because of missing exact temperature ramping data for these measurements.

Figures 7 and 8 are shown to illustrate the supersaturation of self-interstitials caused by the formation of substitutional gold due to reaction (2) and the out-diffusion of self-interstitials to the wafer surfaces. The wafer surfaces maintain the equilibrium concentration of self-interstitials. After 0.5 h at 800° C, the supersaturation ratio C_I/C_I^* is approximately 200 (Fig. 7). With increasing time more and more self-interstitials diffuse to the surfaces and the supersaturation decreases to 60 after 2.0 h and to 25 after 16.0 h. The corresponding supersaturations for 900° C are 60, 20, and 6, respectively (Fig. 8). The concentration of interstitial gold was almost equal to its equilibrium concentration after 0.5 h at 800 and 900° C and, therefore, needs not to be shown.

A variation of the initial self-interstitial concentrations in simulations with (8) to (10) by a factor of 100, respectively of 10^4, to larger values compared to the equilibrium concentration C_I^*, proved that $C_I(t=0)$ has little influence on the substitutional gold concentration and that $C_I(t=0)=C_I^*$ is a reasonable choice. For the factor of 100, C_s in the bulk was reduced by 0.8% and for the factor of 10^4 by 21% at 800° C. At 900° C, the corresponding reductions were 0.3% and 5.8%, respectively.

3.1.2 Boundaries for the Equilibrium Concentration of Self-Interstitials. At the lowest diffusion temperature, diffusion of self-interstitials from the bulk to the surface was still possible. Therefore, it is not possible to obtain a relation between $C_I(t=0)$ and C_I^* or to calculate C_I^* exactly according to (28). It is possible, however, to deduce an upper boundary for C_I^* from our measurements. According to (28), the following considerations can be made. Due to the out-diffusion of self-interstitials, a higher substitutional gold concentration results than would be possible when no out-diffusion occurs. When we calculate for C_I^* the value of 1.5×10^{10} cm^{-3} for the shortest diffusion time of 0.5 h at 800° C with $C_s=3.0\times10^{12}$ cm^{-3} and $C_s^*=6.0\times10^{14}$ cm^{-3} using (28), this value for C_I^* will be larger than for the case where no out-diffusion of I takes place. Analogously for 30 min at 900° C, we obtain an upper boundary of 1.0×10^{12} cm^{-3} with $C_s=6.0\times10^{13}$ cm^{-3} and $C_s^*=3.3\times10^{15}$ cm^{-3}. According to these values of 1.5×10^{10} cm^{-3} at 800° C and of 1.0×10^{12} cm^{-3} at 900° C, C_I^* has to fulfill the condition:

$$C_I^* < 3.72\times10^{31}\exp(-4.55\text{ eV}/kT)\text{ cm}^{-3}. \quad (30)$$

In order to find a lower boundary for C_I^*, simulations with smaller values for C_I^* were performed. D_I was increased by the same factor as C_I^* was reduced in order to keep the product $D_IC_I^*$ constant. Even for a reduction factor of 1000, practically no difference was found in the simulated profiles for C_s in comparison to the profiles shown in Figs. 2 and 3. It can be concluded that a lower boundary for C_I^* cannot be found using such an approach. For a diffusion time of 0.5 h at 800° C, there still was diffusion of self-interstitials observed from the bulk to the surfaces. In order to come into the plateau region, two possibilities can be suggested: to choose shorter diffusion times and/or thicker samples and lower diffusion temperatures. However, the possibility cannot be excluded that the diffusion coefficient of self-interstitials is larger than D_i of gold. Then it will not be possible to use (28) to determine C_I^*

with gold diffusion. A prerequisite to determine C_I^* is that the interstitial diffusion coefficient D_i of an appropriate element is larger than the self-interstitial diffusion coefficient D_I.

3.2 Platinum

3.2.1 Characterization of Diffusion Behavior. The measured bulk platinum concentration after 4.0 h is approximately a factor of 1.4 larger than after 2.0 h at 950° C and 900° C, i.e., at these temperatures C_s in the bulk increases with the square root of time [48]. According to (26), the conclusion can be drawn that the kick-out mechanism dominates at these temperatures. Figure 9 shows measured platinum profiles after diffusion at 950° C. The results for 900° C are shown elsewhere [48]. At 900 and 950° C, the out-diffusion of self-interstitials signs responsible for these platinum profiles.

The platinum profiles which were measured after diffusion at 850° C, 770° C, or 700° C, however, show a quite different shape. The concentration of substitutional platinum in the bulk is approximately the same after the different diffusion times. At 770° C, C_s equals approximately 3.5×10^{13} cm^{-3} after diffusion times of 0.5 and 4 hours (Fig. 10). At 850° C, the measured platinum concentrations also were approximately equal after 0.5 and 4.0 h [48]. Obviously, these diffusion profiles belong to the plateau region of Fig. 1, where no diffusion of point defects from or to the wafer surface takes place. The explanation of the platinum diffusion profiles at 850, 770, and 700° C with the help of the kick-out mechanism can be excluded, because the diffusion coefficient of self-interstitials, as obtained from the gold profiles above, is much too large. Therefore, the conclusion can be drawn that platinum diffuses via the dissociative mechanism at temperatures of 850° C and below. The platinum concentration in the bulk does not rise above the value of C_s^b which can be calculated from (20) and is the same for the different diffusion times. C_s^b is determined by the equilibrium concentration of substitutional platinum, by the initial and by the equilibrium concentration of vacancies according to (20).

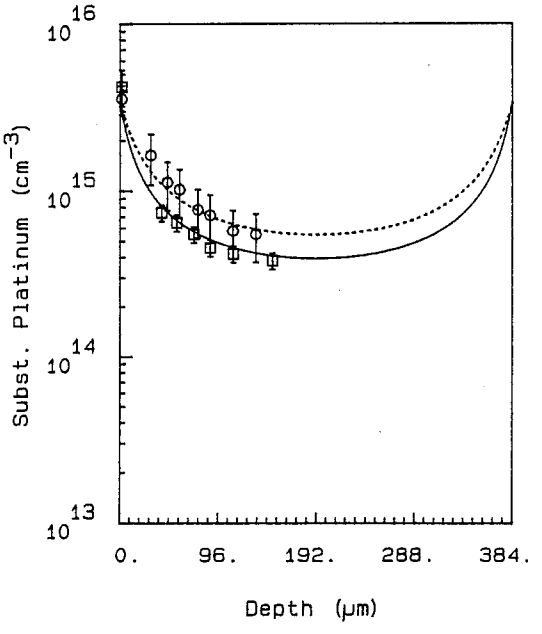

Fig. 9. Measured and simulated platinum profiles after diffusion at 950° C (□: 2.0 h, ○: 4.0 h). The kick-out mechanism is dominating. The initial vacancy concentration in the samples was smaller than 4×10^{14} cm^{-3} ⟨(——) 0.5 h; (- - -) 4.0 h⟩

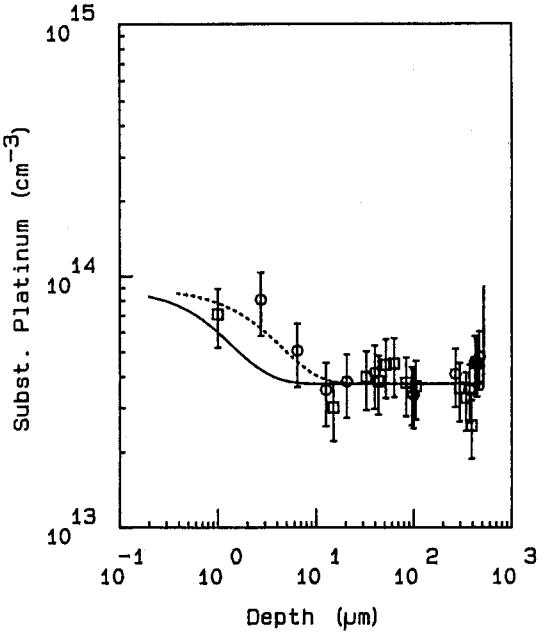

Fig. 10. Measured and simulated platinum profiles after diffusion at 770° C (□: 0.5 h, ○: 4.0 h). The dissociative mechanism dominates. The initial vacancy concentration in the samples was 5.5×10^{13} cm^{-3} ⟨(——) 0.5 h; (- - -) 4.0 h⟩

Equation (20) can also be taken to determine the highest temperature up to which the dissociative mechanism dominates over the kick-out mechanism. If C_s^b calculated from (20) is larger than the concentration of substitutional platinum, which can be formed via the kick-out mechanism (compare (26)), the dissociative mechanism dominates.

Measurements after platinum diffusion at 700° C prove that the initial concentration of the vacancies is not equal to their equilibrium concentration [49]. The concentration of substitutional platinum in the bulk is approximately 1.0×10^{14} cm^{-3} after diffusion times of 4 and 142 hours (Fig. 11). Whereas at the wafer surface, the concentration of substitutional platinum is only approximately 1.5×10^{13} cm^{-3}. Simulations using (4) to (6) show this inverse U-shape only if the initial concentration of vacancies is higher than their equilibrium concentration [28, 49]. In the case when the equilibrium concentration of vacancies is taken as initial value for the simulation, the concentration of substitutional platinum does not rise above the equilibrium concentration of substitutional platinum, which corresponds to the concentration of substitutional platinum at the wafer surfaces. From (21), which holds for $C_V(t=0) = C_V^*$, the condition $C_s^b < C_s^*$ also can be deduced, when (21) is brought into the form $C_s^b = C_V^* C_s^* / (C_V^* + C_s^*)$.

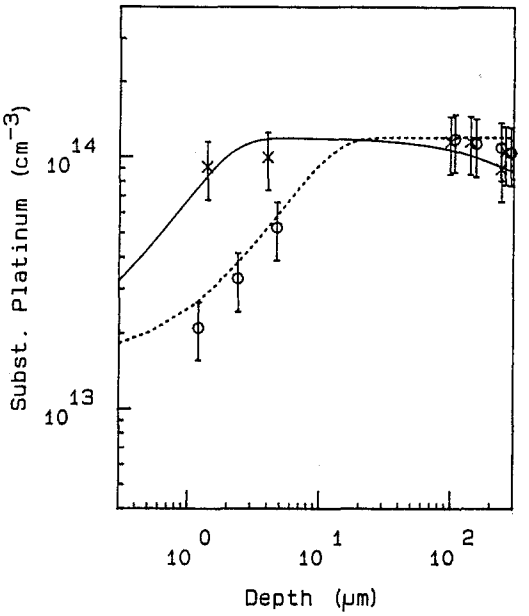

Fig. 11. Measured and simulated inverse *U*-shaped platinum profiles after diffusion at 700° C (×: 4.0 h; ○: 142 h). The dissociative mechanism dominates. The initial vacancy concentration in the samples was 2.2×10^{14} cm^{-3} ⟨(——) 4 h; (- - -) 142 h⟩

The most important conclusion from these inverse *U*-shaped platinum profiles, however, is that vacancies are not present in their equilibrium concentration at low process temperatures. It follows from these inverse *U*-shaped platinum profiles and from the dominance of the dissociative mechanism during platinum diffusion at 700, 770, and 850° C that diffusion processes, which are dominated by vacancies, are governed mainly by the initial concentration of vacancies and not by their equilibrium concentration at least below approximately 850° C.

At 700° C, the initial concentration of vacancies is much larger than their equilibrium concentration. Therefore, the concentration of substitutional platinum becomes higher in the bulk than C_s^* at the wafer surface (Fig. 11). In the past, bulk metal concentrations larger than the surface value C_s^* had not been measured for in-diffusions and for in-diffusions the surface value C_s^* was called substitutional solubility of the metal. These inverse *U*-shaped platinum profiles in Fig. 11, however, show that it is not appropriate to call C_s^* the solubility of substitional platinum. C_s^* has to be defined as the equilibrium concentration of substitutional platinum. These inverse *U*-shaped profiles, furthermore, may serve as the evidence that larger vacancy concentrations than C_s^* can be investigated by means of platinum diffusion.

For the sake of completeness, it shall be mentioned that solutions of the kick-out (8) to (10) also can cause an inverse *U*-shape of C_s-profiles, when $C_I(t=0)$ is chosen appropriately. In order to explain the measured inverse *U*-shaped platinum profiles in terms of the kick-out mechanism, however, a small diffusion coefficient of self-interstitials D_I would be necessary. Gold diffusion profiles, however, showed that D_I is much larger. The inverse *U*-shaped platinum profiles, therefore, can only be explained in terms of the dissociative mechanism.

3.2.2 Point Defect Generation or Recombination. Equation (25) and the platinum profiles of 850, 770, and 700° C can be used to estimate the effectiveness of the generation or recombination of self-interstitials and vacancies. After 4.0 h at 850° C, a platinum concentration of approximately 6×10^{13} cm^{-3} was measured in the bulk. Compared to the concentration of 5×10^{13} cm^{-3} after 0.5 h, this concentration is larger by 1×10^{13} cm^{-3} [48]. If this increase is assumed not to be due to a beginning contribution of the kick-out mechanism, it can be concluded that C_V^* was larger than $C_V(t=0)$ in these samples. When we approximate ΔC_{gr} by $K_B C_I^* C_V^* \Delta t$ (compare Sect. 2.6.1), the term $K_B C_I^* C_V^*$ should be of the order of 10^9 cm^{-3} s^{-1} at 850° C [(25) with $\Delta C_s^b = 1 \times 10^{13}$ cm^{-3}, $\Delta t = 12\,600$ s, and $C_V^* \ll C_s^*$].

At 770° C, ΔC_s^b was smaller than 2×10^{12} cm^{-3}, when we assume that a difference in the platinum concentration between 0.5 and 4.0 h of 5% would be noticeable. $K_B C_I^* C_V^*$ can be estimated to be of the order of 10^8 cm^{-3} s^{-1}. $K_B C_I^*$ can be replaced by K_V, which was estimated to be smaller than 10^{-5} s^{-1} at 770° C [47]. C_V^*, then, has to be of the order of 10^{13} cm^{-3}. With $C_I^* = 10^9$ cm^{-3} [compare (16)], K_B can be estimated to be 10^{-14} cm^{-3} s^{-1} or less.

From the universe *U*-shaped platinum profiles at 700° C, $C_V(t=0) \gg C_V^*$ can be concluded. The term ΔC_{gr}, therefore, can be expressed by $-K_B C_I^* C_V(t=0)$. With $C_V(t=0) = 2.2. \times 10^{14}$ cm^{-3} (see figure caption 11), ΔC_s^b smaller than 5×10^{12} cm^{-3}, and $\Delta t = 511\,200$ s, $K_B C_I^*$ should be smaller than 5×10^{-8} s^{-1}. K_V, which is equal to $K_B C_I^*$, was estimated to be smaller than 10^{-6} s^{-1} [49]. According to the new lower limit, K_B should be of the order of 5×10^{-16} cm^{-3} s^{-1} or smaller, when C_I^* is 10^8 cm^{-3}, instead of lower than 10^{-14} cm^{-3} s^{-1}.

The considerations in this section can be summarized as follows: Practically no change of the measured platinum concentration as a function of time was observed in the plateau region. According to (25), the ineffectiveness of Frenkel pair generation or recombination results.

An interesting and very important conclusion can be drawn from the inverse *U*-shaped profiles and the ineffectiveness of Frenkel pair generation or recombination: it is possible to measure vacancy distributions by means of platinum diffusion according to (20). It shall be mentioned that Frenkel pair generation/recombination does not influence this measurement, because the equilibrium concentration of self-interstitials C_I^* is very small compared to C_V^* and because D_I is large.

3.2.3 Numerical Modeling. According to the dependence of the dominating mechanism on temperature and on the initial vacancy concentration, both diffusion mechanisms have to be taken into account for the modeling of platinum diffusion. Equation (12) to (15) have to be solved simultaneously. The set of parameters (C_i^*, D_i, C_V^*, C_I^*, k_{+1}, and k_{+2}) in (12) to (15) was optimized to fit our platinum diffusion profiles measured with DLTS. The

diffusion coefficients D_V and D_I were calculated from the products $C_I^* \cdot D_I$ and $C_V^* \cdot D_V$ given by Tan [2].

The initial vacancy concentrations for the simulations (700, 770, and 850° C) had not to be fitted: They are related to C_V^* and to be measured quantities C_s^b and C_s^* according to (20). Figure 12 contains the relations between $C_V(t=0)$ and C_V^* for the measured values of C_s^b and C_s^* at 700, 770, and 850° C. Figure 12 also illustrates the circumstance that it is not possible to assume the same initial vacancy concentration for all measured diffusion profiles. When an horizontal line is drawn in Fig. 12, for example at $C_V(t=0)=4\times10^{14}\,\mathrm{cm}^{-3}$, the intersections with the curves for 700, 770, and 850° C do not result in an arrhenius expression for C_V^* However, an arrhenius expression should hold for C_V^*. Therefore, different values for $C_V(t=0)$ result from (20) for the samples from different wafers.

Good agreement between simulated and measured platinum profiles for the temperature range from 700° C to 950° C (see Figs. 9 to 11) is obtained with the following set of parameters [48]:

$$C_s^* = 4.44\times10^{24}\exp(-2.212\,\mathrm{eV}/kT)\,\mathrm{cm}^{-3}, \quad (31\mathrm{a})$$

$$C_i^* = 1.79\times10^{22}\exp(-1.920\,\mathrm{eV}/kT)\,\mathrm{cm}^{-3}, \quad (31\mathrm{b})$$

$$D_i = 5.07\times10^{-2}\exp(-0.604\,\mathrm{eV}/kT)\,\mathrm{cm}^2\,\mathrm{s}^{-1}, \quad (31\mathrm{c})$$

$$C_V^* = 1.83\times10^{19}\exp(-1.162\,\mathrm{eV}/kT)\,\mathrm{cm}^{-3}, \quad (31\mathrm{d})$$

$$D_V = 1.09\times10^{3}\exp(-2.838\,\mathrm{eV}/kT)\,\mathrm{cm}^2\,\mathrm{s}^{-1}, \quad (31\mathrm{e})$$

$$C_I^* = 1.94\times10^{27}\exp(-3.835\,\mathrm{eV}/kT)\,\mathrm{cm}^{-3}, \quad (31\mathrm{f})$$

$$D_I = 2.58\times10^{-2}\exp(-0.965\,\mathrm{eV}/kT)\,\mathrm{cm}^2\,\mathrm{s}^{-1}, \quad (31\mathrm{g})$$

$$k_{+1} = 8.12\times10^{-13}\exp(-0.330\,\mathrm{eV}/kT)\,\mathrm{cm}^3\,\mathrm{s}^{-1}, \quad (31\mathrm{h})$$

$$k_{+2} = 1.50\times10^{23}\exp(-5.200\,\mathrm{eV}/kT)\,\mathrm{s}^{-1}, \quad (31\mathrm{i})$$

$$k_B = 2.80\times10^{7}\exp(-4.910\,\mathrm{eV}/kT)\,\mathrm{cm}^3\,\mathrm{s}^{-1}. \quad (31\mathrm{j})$$

The expression (31 a) for C_s^* is obtained by measurements. Our values lie between the values reported for substitutional platinum by Hauber [18] and Lisiak [50]. The self-interstitial parameters C_I^* and D_I are identical to the parameters used for the modeling of gold diffusion in Sect. 3.1.1. The formulae in the above shown set of parameters for C_i^*, D_i, and the reaction rates k_{+1} and k_{+2} with the activation energies of 1.920 eV, 0.604 eV, 0.330 eV, and 5.200 eV represent only rough estimates. However, they are consistent with (7) and (11), i.e., the activation energies of the reverse reactions are positive as is necessary to fulfil physical reasons.

The value of (31 f) for C_I^* is approximately a factor of 10 smaller than the value of Tan [2] at 1100° C (see Fig. 13). The difference becomes smaller for lower temperatures. Morehead [4] reported almost the same values as can be calculated from our expression for C_I^*. The values of Bronner [3], Boit [5], and Taniguchi [1] are much larger than our values for C_I^*. The values of Boit do not seem to be very reliable, because he admits an error of 10% in the temperature measurement in his rapid optical annealing experiments, and because of the strong influence of the cooling phase. Taniguchi calculated the self-

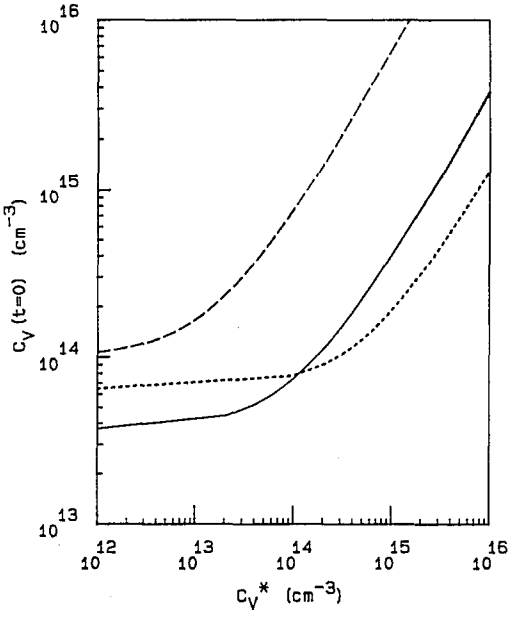

Fig. 12. Relations between initial $C_V(t=0)$ and equilibrium (C_V^*) concentration of the vacancies for measured equilibrium (C_s^*) and bulk (C_s^b) platinum concentrations of the 850, 770, and 700° C diffusion profiles according to (20) ⟨(– – –) 700° C; (——) 770° C; (- - -) 850° C⟩

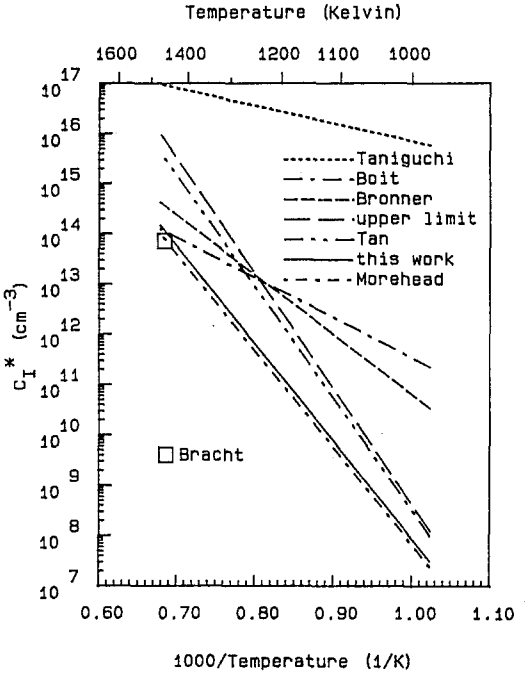

Fig. 13. Comparison of various values for the equilibrium concentration of silicon self-interstitials

interstitial parameters from the growth of oxidation induced stacking faults in the temperature range from 1100 to 1200° C. It also seems possible that traps in the bulk acted as sinks for the self-interstitials. Furthermore, he neglected the influence of vacancies.

Analog to Sect. 3.1.2, simulations of platinum diffusion with (12) to (15) are not very sensitive to different values of

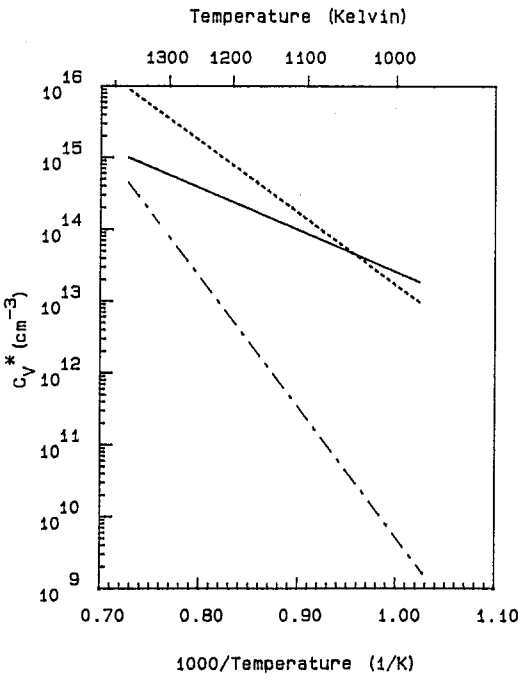

Fig. 14. Comparison of our values for the equilibrium concentration of vacancies with the values of Tan [2] and Dannefaer [6] [(——) this work; (- - -) Tan; (—·—·) Dannefaer]

C_I^*, i.e., to different splittings of the so-called self-diffusion coefficient $D_I \cdot C_I^*$. However, we were able to find an upper limit for C_I^* [see (30)] by means of gold diffusion (Fig. 13). The values for C_I^* (31f), which we used to simulate our measured gold and platinum profiles, are approximately one order of magnitude smaller than the limiting upper values. Actually, it turned out that Bracht et al. [51] used a value of 7×10^{13} cm^{-3} for C_I^* at 1208° C (1481 K) to simulate zinc diffusion profiles. Equation (31f) is in good agreement with this value.

The value of (31d) for C_V^* lies one order of magnitude below the value of Tan [2] at 1100° C (Fig. 14). At approximately 800° C both values for C_V^* are equal. Dannefaer et al. determined C_V^* by means of positron annihilation experiments [6]. The activation energy was found to be 3.6 ± 0.2 eV. However, even after the correct interpretation of their data by VanVechten [52], who calculated a value of 8×10^{13} cm^{-3} at 1300 K (1027° C), the absolute value has an uncertainty of at least one order of magnitude to lower and higher concentrations.

In view of the high accuracy of DLTS measurements and the results of many platinum diffusions, which were performed in the presence of high concentration phosphorus profiles [28], our vacancy parameters should be very reliable for temperatures below about 900° C. With (20) and (21), additionally, the base for the experimental determination of C_V^* has been set and it was shown that C_V^* can be measured accurately, when contamination during long lasting diffusions are avoided [53].

The point defect bulk recombination rate K_B (31j), C_I^* (31f), and C_V^* (31d) are consistent with the product $K_B C_I^* C_V^*$ evaluated by Pichler [54] from boron diffusion during ion implantation at high temperatures. We, however, examined another value for K_B. According to [24], an activation energy of 1.4 eV was assumed for the bulk reaction rate, whereas the preexponential factor was chosen so that at 1000° C, the resulting K_B equals the value given by Budil [55]. The resulting expression $K_B = 3.43 \times 10^{-12} \exp(-1.4\,\text{eV}/kT)$ cm^3 s^{-1} leads to smaller values than the expression (31j). The values for K_B of (31j) are much smaller than the upper boundaries, which were estimated in Sect. 3.2.2. Therefore, the influence of this K_B on the simulated platinum profiles is very small. Simulations even with $K_B = 0$ showed practically no difference compared to the values (31j). The values (31j) for K_B seem to be the most reliable. In order to save computation time in calculating platinum diffusion profiles, it may be reasonable, however, especially in regard of the considerations in Sect. 3.2.2 to set K_B equal to zero.

As a further result, besides a complete set of parameters for the modeling of platinum diffusion, (20) allows the calculation of the initial vacancy concentrations, which were determined by the growth process of the crystals in the case of the diffusion experiments in this paper, because no temperature treatment was performed before platinum diffusion. In the wafers, which were diffused at 950° C, $C_V(t=0)$ can only be estimated to be smaller than 4×10^{14} cm^{-3}, because the dissociative mechanism did not dominate at this temperature. In the samples, which were diffused at 850° C or 770° C, the initial vacancy concentration can be calculated to be 5.5×10^{13} cm^{-3}. The samples, which were diffused at 700° C show an initial vacancy concentration of 2.2×10^{14} cm^{-3}. It can be concluded that the vacancy concentration varies considerably in float zone silicon wafers.

The boron doping concentration was the same for the 770 and 850° C samples and for the diffusion times of 0.5 and 4 h (approximately 1×10^{16} cm^{-3}). In the samples diffused for 4 and 142 h at 700° C, the boron concentration was approximately 6×10^{14} cm^{-3}. From these facts it may be allowed to speculate that the vacancy concentration remains larger for lower boron concentrations during the cooling phase after float zone crystal growth. However, it shall be mentioned that the vacancy concentration could also depend on growth rate, thermal gradients, oxygen, nitrogen, and/or carbon concentrations, which were not determined for our samples.

Our result that platinum diffuses predominantly via the kick-out mechanism at temperatures of 900° C and above is in accordance with the results of Hauber [18], who showed measurements between 1050° C and 1200° C. We can, however, not verify the conclusions of Mantovani et al. [16, 17] who interpreted their DLTS measurements on samples diffused at temperatures between 650° C and 850° C only in terms of the kick-out mechanism even at the lowest temperature of 650° C. A possible explanation is the fact that they used an epitaxially grown silicon layer of approximately 25 μm for their platinum diffusions. Griffin suggested that point defect concentrations are different in float zone, Czochralski, and epitaxial silicon [56]. It can be concluded that the vacancy concentration in the epitaxial layers of Man-

tovani et al. was much lower than in the float zone wafers, which were used in our experiments.

4 Summary

The formation of substitutional gold and platinum was studied analytically, experimentally, and numerically. The DLTS technique was successfully employed for accurate measurements of gold and platinum diffusion profiles in silicon. The gold profiles can be simulated with the three equations of the kick-out mechanism alone. Whereas, the complete set of four differential equations for the kick-out and dissociative mechanisms has to be used for modeling the measured platinum profiles. A complete and consistent set of parameters was suggested which describes the diffusion of gold and of platinum in silicon in the temperature range from 800° C to 1100° C, and from 700° C to 950° C, respectively. It was proposed that for platinum in float zone silicon the kick-out mechanism dominates at approximately 900° C and above, whereas the dissociative mechanism dominates at approximately 850° C and below. An analytical expression was deduced which allows the determination of the exact temperature region for the dominance of the dissociative mechanism.

From measured gold profiles, the conclusion could be drawn that self-interstitials diffuse fast in the examined temperature range and that their equilibrium concentration is small. An upper limit for the self-interstitial equilibrium concentration was found, which reduces the possible range considerably compared to literature values. Platinum profiles showed that vacancies diffuse slowly and that their equilibrium concentration is high. Platinum profiles also induced that the generation and recombination of self-interstitials and vacancies seem to be rather ineffective.

A plateau region in the increase of substitutional metal as a function of time was investigated. This plateau region was found to be the key to the determination of point defect equilibria concentrations. Platinum diffusion was shown to be appropriate to use this plateau region to investigate vacancy distributions quantitatively.

The vacancy concentration was found to be different from the equilibrium concentration at least for temperatures smaller than 850° C and to be determined by the growth process of the crystal. The vacancy concentration varies considerably in float zone silicon wafers. Platinum diffusion, therefore, can be suggested to investigate vacancy distributions accurately after crystal growth. For the first time platinum diffusion offers the possibility to investigate and greatly improve the growth process with respect to vacancy distributions.

Acknowledgements. The authors would like to thank P. Pichler for useful discussions and A. Strauss for carefully performed platinum diffusions. The authors also are indebted to J. Gogl and G. Malieske from Semikron for the gold diffusions. Furthermore, we appreciate the sample preparation and assistance in plotting the results of Th. Klauser. One of the authors (H.Z.) gratefully thanks U. Gösele and T.Y. Tan for the possibility to complete this article as an Alexander-von Humboldt research fellow at Duke University. This work has been supported in part by the 'German Bundesministerium für Forschung und Technology'.

References

1. K. Taniguchi, D.A. Antoniadis, Y. Matsushita: Appl. Phys. Lett. **42**, 961 (1983)
2. T.Y. Tan, U. Gösele: Appl. Phys. A **37**, 1 (1985)
3. G.B. Bronner, J.D. Plummer: J. Appl. Phys. **61**, 5286 (1987)
4. F.F. Morehead: Mat. Res. Soc. Symp. Proc. Vol. **104**, 99 (1988)
5. C. Boit, F. Lau, R. Sittig: Appl. Phys. A **50**, 197 (1990)
6. S. Dannefaer, P. Mascher, D. Kerr: Phys. Rev. Lett. **56**, 2195 (1986)
7. W.C. Dash: J. Appl. Phys. **31**, 2275 (1960)
8. W.R. Wilcox, T.J. LaChapelle: J. Appl. Phys. **35**, 240 (1964)
9. M. Yoshida, K. Saito: Jpn. J. Appl. Phys. **9**, 1217 (1970)
10. F.A. Huntley, A.F.W. Willoughby: Philos. Mag. **28**, 1319 (1973)
11. F. Morehead, N.A. Stolwijk, W. Meyberg, U. Gösele: Appl. Phys. Lett. **42**, 690 (1983)
12. N.A. Stolwijk, B. Schuster, J. Hölzl, H. Mehrer, W. Frank: Physica B **116**, 335 (1983)
13. N.A. Stolwijk, B. Schuster, J. Hölzl: Appl. Phys. A **33**, 133 (1984)
14. N.A. Stolwijk, J. Hölzl, W. Frank, E.R. Weber, H. Mehrer: Appl. Phys. A **39**, 37 (1986)
15. S. Coffa, L. Calcagno, S. Campisano, G. Calleri, G. Ferla: J. Appl. Phys. **64**, 6291 (1988)
16. S. Mantovani, F. Nava, C. Nobili, M. Conti, G. Pignatel: Appl. Phys. Lett. **44**, 328 (1984)
17. S. Mantovani, F. Nava, C. Nobili, G. Ottaviani: Phys. Rev. B **33**, 5536 (1986)
18. J. Hauber, W. Frank, N.A. Stolwijk: Diffusion and Solubility of Platinum in Silicon: Mater. Sci. Forum, Vol. **38–41**, 707 (1989)
19. U. Gösele, W. Frank, A. Seeger: Appl. Phys. **23**, 361 (1980)
20. F.C. Frank, D. Turnbull: Phys. Rev. **104**, 617 (1956)
21. A. Seeger, K.P. Chik: Phys. Status Solidi **29**, 455 (1968)
22. S. Mizuo, H. Higuchi: Jpn. J. Appl. Phys. **20**, 739 (1981)
23. D.A. Antoniadis: J. Electrochem. Soc. **129**, 1093 (1982)
24. D.A. Antoniadis, I. Moskowitz: J. Appl. Phys. **53**, 6788 (1982)
25. T.Y. Tan, U. Gösele, F.F. Morehead: Appl. Phys. A **31**, 97 (1983)
26. U. Gösele, T.Y. Tan: Mat. Res. Symp. Proc. **36**, 105 (1985)
27. Filmtronics Inc., Butler, Pennsylvania 16003, USA
28. H. Zimmermann: Ph.D. thesis, University of Erlangen-Nürnberg, 1991
29. S.M. Sze: Physics of Semiconductor Devices (Wiley, New York 1981) p. 291
30. G. Ferenczi, P. Krispin, M. Somogyi: J. Appl. Phys. **54**, 3902 (1983)
31. M.D. Miller, H. Schade, C.J. Nuese: J. Appl. Phys. **47**, 2569 (1976)
32. S.D. Brotherton, P. Bradley, J. Bicknell: J. Appl. Phys. **50**, 3396 (1979)
33. G. Armelles, J. Barrau, M. Brousseau: Solid State Commun. **56**, 303 (1985)
34. L. Lebedo, Z.-G. Wang: Appl. Phys. Lett. **42**, 680 (1983)
35. J. Utzig, W. Schröter: Appl. Phys. Lett. **45**, 761 (1984)
36. R. Kassing, L. Cohausz, P. v. Staa, W. Mackert, H.J. Hoffman: Appl. Phys. A **34**, 41 (1984)
37. T. Brabec, E. Guerrero, M. Budil, H.W. Pötzl: Z. Phys. B **67**, 415 (1987)
38. M.E. Law, R.W. Dutton: IEEE Trans. CAD-**7**, 181 (1988)
39. R. Dürr, P. Pichler: In: *Simulation of Semiconductor Devices and Processes*, Vol. 3, ed. by G. Baccarani, M. Rudan (Bologna, Tecnoprint 1988) p. 405
40. M.D. Sturge: Proc. Phys. Soc. London **73**, 297 (1959)
41. M. Yoshida, K. Saito: Jpn. J. Appl. Phys. **9**, 1217 (1970)
42. A.J.R. de Kock: Proc. Semiconductor Silicon 1977, Vol. **77-2**, ed. by H.R. Huff, E. Sirtl (The Electrochemical Society, Pennington, NJ 1977) p. 508

43. N.A. Stolwijk, J. Hölzl, W. Frank, J. Hauber, H. Mehrer: Phys. Stat. Sol. (a) **104**, 225 (1987)
44. P. Pichler: Ph.D. thesis, TU Vienna, 1985
45. S.M. Hu: Appl. Phys. Lett. **43**, 449 (1983)
46. J. Crank: The Mathematics of Diffusion (Clarendon, Oxford 1985) p. 22
47. H. Zimmermann, H. Ryssel: Phys. Rev. B **44**, 9064 (1991)
48. H. Zimmermann, H. Ryssel: J. Electrochem. Soc. **139**, 256 (1992)
49. H. Zimmermann, H. Ryssel: Appl. Phys. Lett. **59**, 1209 (1991)
50. K.P. Lisiak, A.G. Milnes: Solid-State Electron. **18**, 533 (1975)
51. H. Bracht, N.A. Stolwijk, H. Mehrer, I. Yonenaga: Appl. Phys. Lett. **59**, 3559 (1991)
52. J.A. Van Vechten: Phys. Rev. B **33**, 2674 (1986)
53. H. Zimmermann: Appl. Phys. Lett. **59**, 3133 (1991)
54. P. Pichler, R. Schork, H. Ryssel: To be published in: 1991 International Workshop on VLSI Process and Device Modeling, Oiso, Japan
55. M.W. Budil, W. Jüngling, E. Guerrero, S. Selberherr, H.W. Pötzl: Simul. of Sem. Dev. and Processes, Proc. of the II. Int. Conf. in Swansea, p. 384 (1986)
56. P.B. Griffin, S.T. Ahn, W.A. Tiller, J.D. Plummer: Appl. Phys. Lett. **51**, 115 (1987)